Journal of Catalysis 265 (2009) 99–108

Contents lists available at ScienceDirect

Journal of Catalysis

journal homepage: www.elsevier.com/locate/jcat

Bifunctional conversion of *n*-decane over HPW heteropoly acid incorporated into SBA-15 during synthesis

B.C. Gagea, Y. Lorgouilloux, Y. Altintas, P.A. Jacobs, J.A. Martens *

Centre for Surface Chemistry and Catalysis, Katholieke Universiteit Leuven, Kasteelpark Arenberg 23, B-3001 Heverlee, Belgium

ARTICLE INFO

Article history:
Received 12 January 2009
Revised 1 April 2009
Accepted 21 April 2009
Available online 23 May 2009

Keywords:
n-Decane hydroisomerization
Heteropoly acids
SBA-15 synthesis
Tungsten phosphoric acid
Bifunctional catalysis

ABSTRACT

SBA-15 ordered mesoporous silica materials containing up to 40 wt.% of HPW heteropoly acid were synthesized via an original method involving the introduction of HPW in an acidified solution of P123 triblock copolymer ($EO_{20}PO_{70}EO_{20}$), the SBA-15 mesostructuring agent (direct synthesis). Samples with similar HPW loadings were also prepared by impregnation of SBA-15. Characterization by XRD, ^{31}P MAS NMR, NH_3-TPD, and N_2 adsorption showed that even after calcination HPW in the direct synthesis samples was better dispersed than that in the impregnated samples. SBA-15-supported HPW materials were converted into bifunctional catalysts. In the conversion of *n*-decane, direct synthesis samples were superior to impregnated samples. The criteria of ideal bifunctional catalysis were fulfilled, e.g. high yields of skeletal isomers (>70%), of multi-branched skeletal isomers, and of branched cracked products, and hydrocracking reactions limited to primary cracking. Compared to ultrastable Y zeolites, the HPW/SBA-15 samples showed a broader optimum reaction temperature window for isomerization and higher *n*-decane dibranching selectivity.

1. Introduction

The acid forms of heteropoly oxometalates designated as heteropoly acids (HPAs) are known for their strong BrØnsted acid properties that are useful for acid catalysis [1–3]. The most popular heteropoly acids are those having the Keggin structure, e.g. $H_3PW_{12}O_{40}$ (HPW). Heteropoly acids are readily soluble in water and polar organic liquids, and have been applied successfully in homogeneous catalysis. Catalyst recovery from the reaction products sometimes can be achieved by using biphasic reaction conditions, and recovery of HPA can be achieved via the aqueous phase. In less polar media where HPA is poorly soluble, the catalytic activity of HPA is limited owing to the low specific surface area exposed by solid HPA particles. Much effort has already been invested in the development of heterogeneous HPA catalysts with the aim to combine the favorable catalytic properties of dissolved HPA with the technical advantages related to the handling of a solid catalyst. One way to heterogenize HPA for use in polar media is by using Cs^+ salts of HPA which are poorly soluble and form porous structures [4]. Another approach to heterogenize HPA is by making use of a non-porous support such as ZrO_2 [5,6] or TiO_2 [7,8], or a porous support such as silica gel, zeolite Y, ordered mesoporous silica (e.g. SBA-15 or MCM-41), or cellular foam silica [9–25]. Halligudi et al. supported HPA on ZrO_2 nanoparticles that were embedded inside the mesopores of SBA-15, MCM-41, or MCM-48 [26,27].

One possible route to obtain these supported HPA catalysts is the direct impregnation of the support with a heteropoly acid solution followed by evaporation of the solvent [9,12,23,24]. Incorporation of HPA into the mesopores can also be achieved via vacuum impregnation [13]. Leaching of HPA from ordered mesoporous silica in polar reaction media can be prevented by surface modification of the support. The deposition of basic alumina clusters; doping of the silicate with Ti, Zr, or Al atoms; and functionalization of the silicate walls with aminosilane groups for anchoring the HPA molecules were reported to be successful [13–17]. Incorporation of HPA into the pores of a mesoporous material can also be achieved by encapsulating HPA during the synthesis of the silica material itself [19–22]. Indeed, Yang et al. incorporated HPW into SBA-15 carrier by adding HPW to the SBA-15 synthesis mixture [20]. Toufaily et al. published a similar approach to incorporate HPW into MSU-type ordered mesoporous silica [22]. Shi et al. obtained SBA-15-supported HPW (or HPMo ($H_3PMo_{12}O_{40}$)) catalysts by adding P and W (or Mo) sources into the initial sol–gel system during hydrolysis of tetraethyl orthosilicate to form the Keggin-type HPA in situ [19,21].

The majority of the published investigations on acid catalysis over HPAs have dealt with heterogeneous catalysis under liquid-phase reaction conditions [1–3]. The moderate thermal stability of heteropoly acids imposes an upper limit on the reaction temperatures for vapor phase applications [20,28]. Several studies on HPA supported on high surface area solids have reported the existence

* Corresponding author. Fax: +32 (0) 16238783.
E-mail address: Johan.Martens@biw.kuleuven.be (J.A. Martens).

0021-9517/$ - see front matter © 2009 Elsevier Inc. All rights reserved.
doi:10.1016/j.jcat.2009.04.017

of an optimum HPA loading in order to obtain the maximum catalytic activity [23,24]. Higher loadings resulted in a lower catalytic activity due to HPA agglomeration. Furthermore, the optimum HPA loading varies depending on the exact preparation procedure and the studied reaction.

Skeletal isomerization of *n*-alkanes in the vapor phase is an application where the strong BrØnsted acidity of HPAs potentially is of particular interest. The stronger the acidity of the catalyst, the lower the reaction temperature required for achieving the chemical reaction. The lower the temperature is, the more the internal thermodynamic equilibrium of the mixture of the *n*-alkane and its skeletal isomers is in favor of the branched isomers, and the further the conversion of the *n*-alkane into skeletal isomers theoretically can proceed. The hydroisomerization of C_4-C_8 *n*-alkanes over bifunctional silica-supported HPA catalysts and acidic cesium salts of $H_3PW_{12}O_{40}$ has been investigated [29–40]. Among the *n*-alkanes, the isomerization of *n*-butane is particularly demanding because of the involvement of primary alkylcarbenium ions in the monomolecular skeletal rearrangements [41]. The strong acidity of HPA can be exploited to achieve this demanding reaction. In the conversion of *n*-hexane, the efficiency of bifunctional HPA catalysts was illustrated by their high activity compared to alternative catalysts such as zeolites [32]. However, longer *n*-alkanes have a tendency to crack besides hydroisomerizing. In the conversion of *n*-octane and longer *n*-alkanes, the realization of an adequate balance between the hydrogenation–dehydrogenation function provided by noble metal and the acid function provided by HPA is critical, and is not easily achieved [40]. An excess of acidity is at the origin of hydrocracking of the carbon chains. Hitherto, the potential of bifunctional HPA-based catalysts for skeletal isomerization and hydrocracking of *n*-alkanes longer than *n*-octane has not been assessed.

Nowadays, there are important challenges in the area of hydroisomerization and hydrocracking of long-chain *n*-alkanes produced in Fischer–Tropsch processes [42]. Hydroisomerization in the absence of cracking is targeted in hydroisomerization–dewaxing processes, and in processes that are employed for the improvement of low temperature properties of diesel, kerosene, and heavier fractions. When using a large-pore bifunctional zeolite catalyst such as Pt- or Pd-loaded ultrastable Y zeolite presenting little molecular shape selectivity, the yield of skeletal isomers is limited because of the occurrence of hydrocracking consecutive to hydroisomerization [43,44]. Over medium-pore type zeolites such as ZSM-22, high yields of skeletal isomerization can be obtained [45–47], but the side chains that are formed are methyl groups only, while for lubricating and pour point lowering, longer side chains would be more advantageous. Another challenge consists in maximizing the cracking in the middle of very long hydrocarbon chains [42]. Since the worldwide need for diesel fuel is steadily increasing, maximization of the yield of molecules in the appropriate carbon number range obtained via systematic cracking near the middle of the chains of very long-chain paraffins produced via Fischer–Tropsch synthesis would present a major advantage. However, during catalysis over noble metal-loaded ultrastable Y zeolite, mechanistically there is little difference in the cracking selectivity among the fifth and more central carbon–carbon bonds in a long alkyl chain [48].

In view of these challenges in the area of hydroisomerization and hydrocracking, we synthesized bifunctional SBA-15-supported HPW catalysts via an original method involving addition of the HPW to the acidified tri-block copolymer solution prior to the addition of the silica source to enhance HPW dispersion. We investigated the hydroisomerization and hydrocracking of *n*-decane over platinum-loaded HPW/SBA-15 catalysts by using it as a model long-chain *n*-alkane.

2. Experimental

2.1. Catalyst preparation

SBA-15 samples were synthesized following a previously published method using the P123 tri-block copolymer ($EO_{20}PO_{70}EO_{20}$) as a structure directing agent [49]. After the hydrothermal step, samples were thoroughly washed with distilled water and were dried at 60 °C for 24 h. Calcination was performed in air at 500 °C for 6 h with a heating ramp of 2 °C/min. Dodecano tungsten phosphoric acid ($H_3PW_{12}O_{40}$ – HPW) was dispersed on the silica support either using an aqueous incipient wetness impregnation technique or via a direct synthesis method.

The aqueous incipient wetness impregnation technique was previously employed by many authors for the immobilization and dispersion of HPA on high surface area supports [9,12,23,24]. The method applied in our case consisted of dissolving hydrated HPW into an appropriate amount of water in order to fill the pores of the calcined SBA-15 sample. Typically, a water volume of 2.5 ml was used per gram of freshly calcined SBA-15. The impregnated samples were dried in two steps: first at 60 °C for 12 h and then at 100 °C also for 12 h. The resulting HPW/SBA-15 samples prepared via impregnation are denoted as *x*%HPW-IMP (where *x* represents the wt.% of anhydrous HPW on dry SBA-15 support).

Incorporation of HPW via the direct synthesis route was achieved via the following adaptation of the SBA-15 synthesis procedure. P123 polymer, 1.92 g ; 40 g of water; and 30 g of HCl (4 M) were mixed following the standard method for SBA-15 synthesis. The necessary quantity of hydrated HPW was dissolved in 5 g of water and was added dropwise under vigorous stirring into the polymer solution. The addition of HPW to the P123 polymer changed the aspect of the solution, and rendered the solution opaque. At HPW loadings lower than 20 wt.%, the P123-HPW compound was still in suspension. Above 20 wt.% HPW, continuous stirring was needed to avoid sedimentation. The mixture was stirred for 24 h before addition of 4 g tetraethyl orthosilicate (TEOS). During hydrolysis of TEOS a white precipitate was formed. After stirring for another 30 min, the mixture was loaded in an autoclave and was heated for 24 h in a furnace heated at 80 °C without additional stirring. The autoclave was cooled, and the product was separated by filtration, washed with deionized water, and dried first at 60 °C and further at 100 °C for 12 h. The calcination step was performed in air at 500 °C for 6 h using a heating ramp of 2 °C/min. The resulting HPW/SBA-15 samples were labeled as *x*%HPW-DS (where *x* represents the wt.% of anhydrous HPW on dry SBA-15, and DS refers to the direct synthesis method).

2.2. Conventional zeolite samples

The following commercial zeolite samples were used: CP811 (H-β zeolite; Si/Al = 12.5); CBV1502 (H-ZSM5; Si/Al = 75); CBV600 (H-USY; Si/Al = 2.8); CBV712 (H-USY, Si/Al = 5.8); CBV720 (H-USY, Si/Al = 13); CBV760 (H-USY, Si/Al = 30); CBV780 (H-USY, Si/Al = 37), supplied by PQ; and PY-44/1C (H-Y, Si/Al = 2.7) obtained from Zeocat. The indicated Si/Al atomic ratio is according to the manufacturer. For the H-USY zeolite series, it was determined by ICP analysis [50].

2.3. High-throughput testing

n-Decane hydroisomerization experiments were performed using a high-throughput reactor with 16 parallel reactor tubes [51]. Before the catalytic experiment, samples were impregnated with aqueous $[Pt(NH_3)_4]Cl_2$ solution to obtain a 0.5 wt.% noble metal loading. The impregnated materials were dried at 60 °C.

Catalyst pellets were obtained by compressing the powder into flakes, crushing the flakes, and sieving to obtain a pellet size of 125–250 μm. Amounts of 50 mg of catalyst were loaded into the reactors and were activated in situ at 400 °C for 1 h first under O_2 and then under flowing H_2. For the conversion of *n*-decane, a fixed contact time of 1.656 kg s/mol was used. The reaction temperature was increased in steps of 10 °C. The total pressure was 0.45 MPa, and the hydrogen to hydrocarbon molar ratio was 375. Product analysis was performed by gas chromatography using a Interscience GC 8000 device equipped with a multi-capillary column (Alltech, Multicap MC-1 ht), containing a bundle of 900 capillaries, with an internal diameter of 40 μm, a length of 1 m, and coated with a 0.2 μm thick film of a non-polar stationary phase (100% dimethyl polysiloxane). Nitrogen was used as a carrier gas with a flow of 67 ml/min. Temperature ramping of the GC oven was from 40 to 75 °C at 15 °C/min.

2.4. Characterization techniques

XRD was performed on a STOE StadiP diffractometer with Cu K_α radiation. Particle size and morphology were analyzed by scanning electron microscopy (SEM) with a JXA-733 JEOL on gold-plated samples. Nitrogen adsorption experiments at -196 °C were carried out with a three-port TRISTAR 3000 apparatus from Micromeritics. All samples were pretreated under N_2 flow for 12 h at 200 °C before the measurement. Quantitative ^{31}P MAS NMR spectroscopy allowed to determine the exact amount of occluded HPW molecules and to characterize the stability of HPW during calcination of the HPW/SBA-15 samples. The spectra were recorded on a Bruker AMX 300 spectrometer. The recording conditions were frequency = 121.4 MHz; recycle time = 20 s; pulse width = 2.0 μs; and pulse angle = 90°, with ^{31}P chemical shifts being referenced to an aqueous solution of H_3PO_4.

To characterize the acidity of the samples, NH_3 temperature-programmed desorption (NH_3-TPD) measurements were carried out. After pretreatment of 75 mg samples in He (400 °C, 20 ml/min, 1 h), the samples were exposed to ammonia at 100 °C for 0.5 h and were then purged with helium for 1 h. NH_3-TPD spectra were registered between 100 and 750 °C (temperature ramp: 10 °C/min) by monitoring the desorbed ammonia with a Pfeiffer Omnistar quadrupole mass spectrometer.

3. Results and discussion

3.1. Synthesis and characterization of HPW catalysts

Many previous studies concerning the supported heteropoly acids revealed the strong agglomeration tendency of the heteropoly acid molecules [13,24]. A direct synthesis (DS) method for the incorporation of HPW in the SBA-15 matrix was conceived in order to attempt better dispersion of HPW. This direct synthesis route was inspired by the proposed supramolecular mechanism of SBA-15 formation [52]. The SBA-15 synthesis is considered to follow a $S^0H^+X^-I^+$ mechanism in which S^0, H^+, X^-, and I^+ stand for P123 tri-block copolymer, hydronium cations, anions (Cl^-), and the positively charged silica source at pH <2, respectively (Scheme 1) [53]. In aqueous solutions, P123 copolymer forms micelles that are usually regarded as containing a hydrophobic core constituted by the propoxy blocks, and a hydrophilic shell of ethoxy groups. Following the addition of a concentrated aqueous HCl solution, the ethoxy groups of P123 are protonated by the H_3O^+ ions conferring a positive charge to the P123 micelles. This positive charge is neutralized by the Cl^- anions present in the reaction mixture. During this stage, the P123 micelles are stabilized and the phase is controlled by the temperature and the pH of the reaction mixture. Due to the very low pH of the reaction medium, just after its incorporation in the synthesis mixture, the TEOS silica source is rapidly hydrolyzed and protonated to yield $H_5SiO_4^+$ monomers. These silicate cations can interact with the chloride anions compensating for the positive charges of the P123 micelles via electrostatic forces, leading to the formation of a silica layer around the P123 micelles.

In the DS method, an appropriate amount of HPW is introduced in the polymer system after addition of HCl. At that point during the synthesis, the P123 template is already positively charged, with the charge being compensated by the chloride anions (Scheme 1). $H_3PW_{12}O_{40}$ is a very strong acid having negative Hammet acidity functions in aqueous solutions for all three dissociation steps [2]. Due to this strong acidity, HPW occurs in the form of the associated weak base. The PW^{x-} anions can substitute the Cl^- anions in the shell surrounding the P123 micelle. The long time of 24 h allowed for this equilibrium to be established ensured that most of the heteropoly anions are attached and molecularly dispersed on the P123 micelle before the addition of the silica source. When TEOS is finally added, it will hydrolyze and transform into the protonated monomers due to the very low pH. The $H_5SiO_4^+$ cations will interact with the anionic shell surrounding the P123 micelle, thus trapping both Cl^- and heteropoly anions between P123 and the silica. During the hydrothermal treatment the silica layer is polymerized. The formation of Si–O–Si bonds strengthens the walls and the mesopore structure. The heteropoly anions will be present at the interface between the silica and the P123 polymer. Washing and drying steps do not remove the heteropoly anions since they are trapped inside the SBA-15 particles. In the calcination step, the P123 template decomposes and is eliminated from the pore system but the HPW molecules stay fixed onto the pore walls.

Other researchers prepared SBA-15-supported HPW catalysts by direct incorporation of HPW during the synthesis of the ordered mesoporous silica material [19,20]. There are some important differences between those synthesis procedures and ours. The main difference is related to the timing of the introduction of HPW. We introduced HPW before the hydrolysis of TEOS for the reasons explained (Scheme 1), whereas in Refs. [19,20] TEOS was already present and had reacted prior to HPW addition. Shi et al. introduced P and W sources (Na_2WO_4 and Na_2HPO_4) instead of HPW in the synthesis mixture. Thus, HPW was formed in situ in the SBA-15 synthesis mixture.

The model for the DS synthesis presented in Scheme 1 predicts that the HPW molecules are well dispersed in the final material, and that they may even be partially embedded in the pore walls.

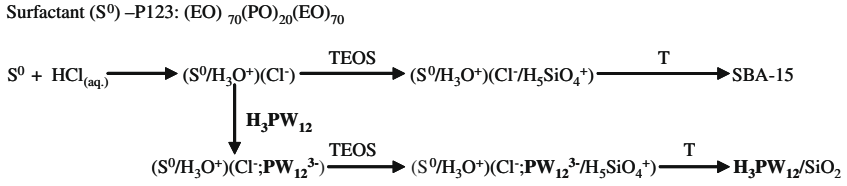

Scheme 1. Proposed synthesis mechanism for *x*%HPW-DS samples (T stands for heating).

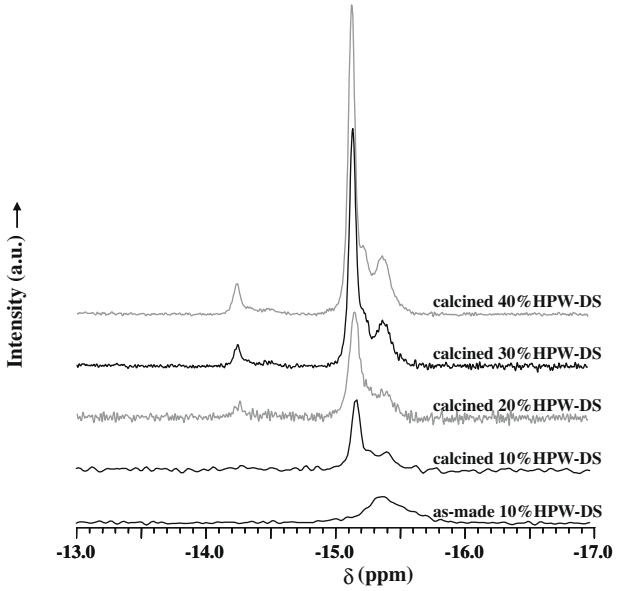

Fig. 1. ^{31}P MAS NMR spectra of calcined HPW-DS samples with different HPW contents and of as-made 10 wt.% HPW-DS sample.

This proposed HPW incorporation mechanism is supported by the high thermal stability of the resulting materials. While pure HPW and HPW in impregnated samples undergo partial decomposition at temperatures as low as 400 °C [54], the HPW-DS samples showed no sign of decomposition after calcination at 500 °C. At 700 °C, some decomposition was detected. Decomposition is evident even to the eye, when materials change color from white to greenish because of the formation of tungsten oxides.

Quantitative ^{31}P MAS NMR spectroscopy was applied on the calcined samples to verify the stability of the HPW-DS samples after calcination at 500 °C (Fig. 1). Resonances around −30 ppm (outside the chemical shift range shown) which are characteristic of P–O–P linkages and would indicate the decomposition of the Keggin ions and the formation of phosphorous oxide [55] were not observed. The spectra of all the four samples (10–40%HPW-DS) contained three signals at −14.3, −15.2, and −15.4 ppm, respectively. Before calcination, the −15.4 ppm resonance was present as the only signal, as shown for 10%HPW-DS (Fig. 1). According to the literature [12,18,56,57], the three resonances in the calcined samples can be attributed to HPW units that have various interactions with the support. The actual concentration of HPW in the samples was estimated by running pure HPW reference sample under identical conditions and by integration of the ^{31}P MAS NMR signal. According to ^{31}P NMR, the samples with nominal HPW content of 10, 20, 30, and 40 wt.% contained 12.2, 20.8, 31.5, and 41.9 wt.% of HPW, respectively, which is in good agreement.

The differences in HPW aggregation on the SBA-15 supports following the two synthesis methods were evidenced by XRD (Fig. 2). All materials showed the characteristic [100] diffraction peak of the hexagonal mesostructure of SBA-15. For the 10 and 20%HPW-DS samples, the [110], [200], [220], and [300] diffraction peaks of hexagonally ordered mesoporous material were observed (see inset Fig. 2A). The low-angle diffractions in the XRD pattern were little intense for the 30 and 40%HPW-DS samples. Second and higher order reflections could no longer be observed in the 40%HPW-DS sample. Although absorption of X-rays by the heavy W element can be responsible for the weaker intensity of the XRD pattern, the less intense XRD pattern of the 40%HPW-DS sample especially points at poorer mesoscale ordering in materials with high HPW content. The high-angle region did not show the

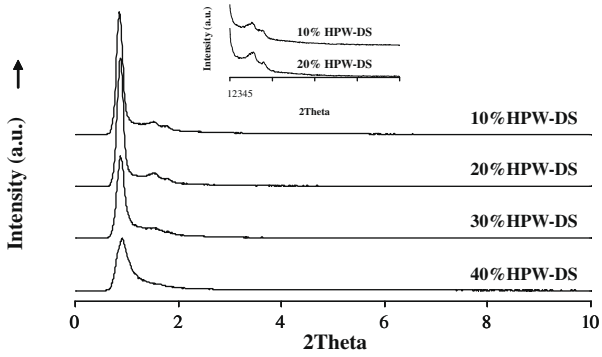

Fig. 2A. Low-angle XRD patterns of HPW-DS samples with different HPW contents.

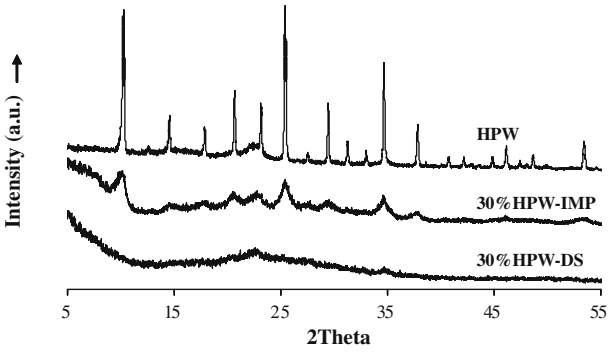

Fig. 2B. High-angle XRD patterns of pure HPW and SBA-15 materials modified with 30 wt.% HPW via the IMP and DS methods.

characteristic diffraction pattern of crystalline HPW phase, not even for the heavily loaded 40%HPW-DS sample, which is an evidence of the dispersed nature of HPW in HPW-DS samples. On the contrary, samples prepared by the impregnation of HPW onto SBA-15 presented the characteristic XRD pattern of crystalline HPW at high loadings (Fig. 2B).

Nitrogen adsorption isotherms for the HPW-DS samples are presented in Fig. 3. For the 10 and 20%HPW-DS samples, the shapes of the isotherms were similar to the one of the SBA-15 carrier material. The main part of the hysteresis loops remained in the same relative pressure range. For the 30 and 40%HPW-DS samples, the desorption branch extended to a lower relative pressure suggesting a partial loss of structural organization and the formation of some narrower pores. Nevertheless, the main part of these hystereses were still between P/P° values of 0.6–0.75. The results

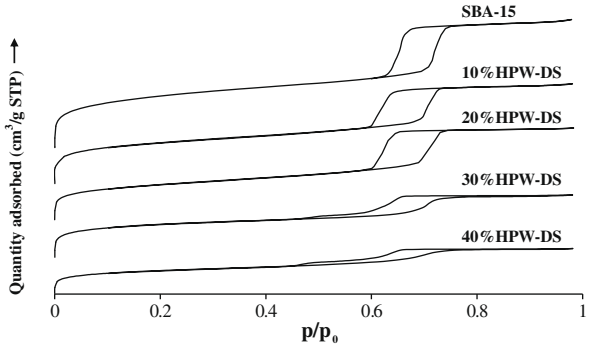

Fig. 3. Nitrogen adsorption isotherms of SBA-15 and HPW-DS samples with different HPW contents.

Table 1
Textural properties of HPW containing SBA-15 materials.

Catalyst	BET (m^2/g)	BET_N[a] (m^2/g)	$V_{mp.}$[b] (cm^3/g)	V_T[c] (cm^3/g)	V_{TN}[a] (cm^3/g)	$d_{mesopore}$ (nm)
SBA-15	1005	1005	0.21	1.09	1.09	5.8
10%HPW-DS	801	890	0.18	0.85	0.94	5.5
20%HPW-DS	699	873	0.16	0.79	0.99	5.5
30%HPW-DS	628	897	0.25	0.53	0.76	5.9
40%HPW-DS	446	743	0.18	0.38	0.63	5.8
10%HPW-IMP	632	702	0.18	0.61	0.68	5.1
20%HPW-IMP	513	641	0.14	0.53	0.66	5.0
30%HPW-IMP	458	654	0.15	0.46	0.66	5.1
40%HPW-IMP	377	628	0.13	0.39	0.65	5.1

[a] Values are normalized per gram of SBA-15 support.
[b] Micropore Volume as determined by *t*-plot and normalized per gram of SBA-15 support.
[c] Total pore volume.

obtained from the textural analysis of the samples based on nitrogen adsorption are presented in Table 1. The total pore volume (V_T) decreased with increasing HPW loading (Table 1). This is logical since the heteropoly acid contributes to the sample weight. The microporosity of the DS samples varied in a non-systematic way with HPW loading in the range 0.18–0.25 cm^3/g. The SBA-15 reference material has a microporosity of 0.21 cm^3/g (Table 1). Micropores in SBA-15 originate from a perfusion of the silica walls with polymer chains, which upon evacuation leave micropores. In DS materials, the formation of micropores likely proceeds in the same way. The packing of the Keggin HPW units can be an additional source of microporosity.

The mesopore size distribution was derived from the desorption branch of the nitrogen physisorption isotherms using the BJH method (Fig. 4). The 30%HPW-DS sample and the SBA-15 sample synthesized in the absence of HPW have about the same mesopore diameter (slightly smaller than 6 nm). It has to be noted that the contributions around 3.8 nm in the pore size distributions of 30%HPW samples shown in Fig. 5 are artifacts caused by the tensile strength effect, and should not be taken into consideration as no corresponding peak is present in the BJH pore size distributions derived from the adsorption branches [58]. All HPW-DS samples have pore sizes around 5.5–5.9 nm, similar to the SBA-15 reference, viz. 5.8 nm (Table 1). In the DS synthesis method, the size of the majority of mesopores is not affected by the presence of HPW (Fig. 4), which is in agreement with the proposed synthesis model (Scheme 1) in which the pore size is imposed by the P123 micelles, which have the same diameter in the presence and absence of HPW. On the contrary, impregnation of the calcined SBA-15 sample with HPW resulted in a reduction of the mesopore diameter to ca. 5 nm (Fig. 4), which shows that HPW inside the mesopores occupies space and decreases the pore width.

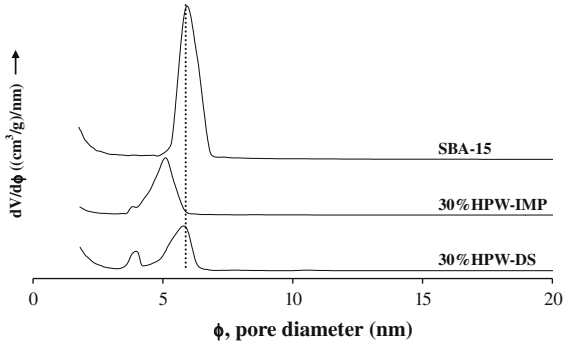

Fig. 4. BJH pore size distributions derived from the desorption branches of the isotherms of pure SBA-15 and SBA-15 materials modified with 30 wt.% HPW via the DS and IMP methods (the dashed vertical line indicates the pore diameter value 5.9 nm).

Nitrogen adsorption experiments revealed a significant loss in surface area for samples prepared using the impregnation technique (Table 1). The IMP samples have a specific surface area of 628–702 m^2/g depending on HPW loading, which is significantly lower than that of the unmodified SBA-15 (1005 m^2/g). The DS samples have a higher specific surface area of 743–897 m^2/g. The loss of surface area upon HPW loading using impregnation has already been reported by other authors [23]. This loss of specific surface area can be related to the agglomeration of HPW molecules on the external surface of the material resulting in pore blockage.

The HPW incorporation method has an impact on the morphology of the resulting HPW/SBA-15 composite (Fig. 5). The impregnated sample with 30 wt.% HPW loading retains a typical SBA-15 morphology, showing chains of grain-type SBA-15 particles with a 0.5–1 μm grain size. The DS sample has a different morphology with irregular particle size, and particle dimensions of up to 5 μm confirming that the HPW had an impact on the formation process of the mesoporous material. The influence of synthesis parameters on the morphology of SBA-15 particles has been studied by Zhao et al. [59]. In particular, they showed that the shape of SBA-15 particles is dependent on the local curvature energy that is present at the interface of the inorganic silica and amphiphilic block copolymer species [59]. In our model (Scheme 1), the HPW molecules are present at this SiO_2–P123 interface and may thus lead to some variation of the curvature energy, which could explain the formation of SBA-15 grains with different morphologies in the presence of HPW.

The acidity of the SBA-15-supported HPW catalysts was characterized by NH_3 temperature-programmed desorption (NH_3–TPD). The NH_3–TPD curves of the four samples synthesized with the DS method display only one wide peak from 150 to approximately 500 °C, with a maximum desorption rate at about 230 °C (Fig. 6). Thus, it seems that there is a broad spectrum of acidities in these HPW-DS materials. The NH_3–TPD of the 40%HPW-IMP sample is displayed in Fig. 7. Ammonia desorption maxima are observed around 210, 410, and 580 °C, respectively. On the HPW-IMP sample compared to HPW-DS, the share of ammonia desorbing at higher temperatures is more important. NH_3–TPD reveals that HPW adopts a different molecular organization in HPW-IMP and HPW-DS samples. The stronger acidity in HPW-IMP samples reveals that the intrinsic acidity of the HPW phase is better maintained. The weaker average acidity of the HPW-DS samples is to be expected from the isolation of the HPW units in the silicate walls and the strong interaction with the silica. For a more detailed characterization of acidities in DS samples in comparison with IMP samples, microcalorimetry and ^1H NMR might be useful [60–62].

The relative concentrations of acid sites obtained by integration of the ammonia desorption signal and normalized to 1.00 for the

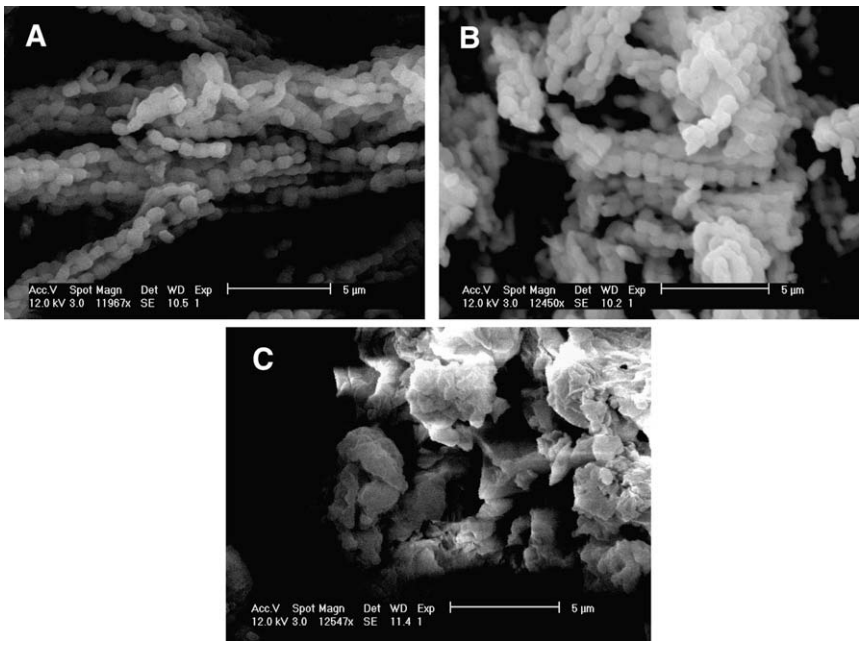

Fig. 5. SEM pictures of (A) SBA-15; (B) 30%HPW-IMP; and (C) 30%HPW-DS samples.

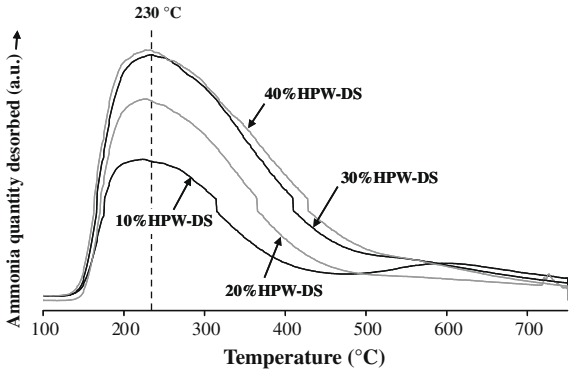

Fig. 6. Temperature-programmed desorption of ammonia from HPW-DS samples with different HPW contents.

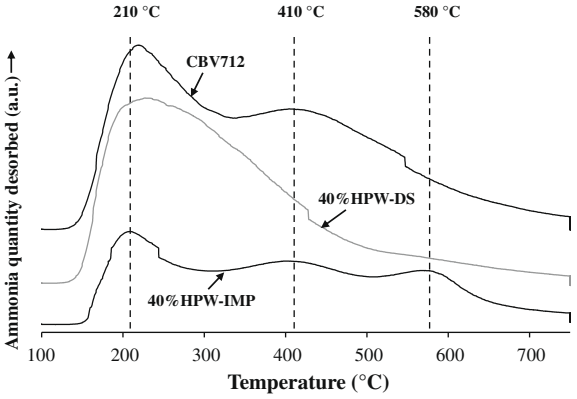

Fig. 7. Temperature-programmed desorption of ammonia from 40 wt.% HPW samples prepared via the DS and IMP methods and from a reference ultrastable Y zeolite sample (CBV712, Si/Al = 5.8).

10%HPW-DS sample are 1.34, 1.75, and 1.85 for 20, 30, and 40%HPW-DS samples, respectively. The acid site concentration does not increase in proportion to the HPW content. It can be concluded from these values that not all acid sites provided by the HPW are available for ammonia adsorption. The inaccessibility of some of the acid sites in the DS samples could be linked with the embedding of HPW in the silica walls. The acidity according to NH_3–TPD of 40%HPW-IMP and DS samples is compared with an ultrastable Y reference zeolite in Fig. 7. The IMP catalyst has relatively more acid sites desorbing ammonia at high temperature. The relative acid site concentration of 40%HPW-IMP sample amounts to 1.17, which is lower than that of the 40%HPW-DS sample. This lower value probably is due to the more significant agglomeration of HPW when introduced in SBA-15 through impregnation. The 40%HPW-DS sample according to NH_3–TPD has some similarity with CBV-712, an ultrastable Y zeolite with a framework Si/Al of ~6 and extra framework aluminum.

In conclusion, following the DS preparation procedure, HPW contents of up to 40 wt.% could be realized in the pores of SBA-15. In the literature, the highest HPW content on the SBA-15 material obtained using an alternative reactant addition sequence was around 23.2 wt.% [19,20].

3.2. Catalytic experiments

For the assessment of the catalytic activity of the SBA-15-supported HPW heteropoly acids, the materials were transformed into bifunctional catalysts. The calcined samples were loaded with 0.5 wt.% of dispersed platinum. The chosen test reaction was *n*-decane hydroisomerization/hydrocracking. From the product selectivity of this particular conversion, much information on the balance between acidity and hydrogenation–dehydrogenation function as well as on the pore architecture can be extracted [63,64]. The role of the metal function, according to the classical bifunctional reaction mechanism, is to rapidly realize hydrogenation/dehydrogenation equilibrium among alkanes and alkenes. The initial reaction step is the dehydrogenation of the alkane on the noble metal site. The formed olefins are protonated by the acid sites (HPW) and are transformed into alkylcarbenium ions. These carbocations are isomerized on the acid sites via a substituted protonated cyclopropane intermediate. Skeletal isomerization is a

stepwise process leading to the formation of di- and tri-branched isomers. The branched alkylcarbenium ions can be cracked via a β-scission mechanism resulting eventually in *n*- and isoalkane reaction products with a carbon number that is lower than that in the feed [41]. When the catalytic functions are well balanced, the reaction selectivity and catalyst activity according to the bifunctional mechanism are independent of the concentration and the dispersion of the noble metal. In bifunctional catalysis, the concentration of alkene intermediates is always low. In non-ideal catalysts, polymerization of alkenes on acid sites may lead to coke formation and to the deactivation of the catalyst.

Previous studies on 1-butene isomerization on supported HPA catalysts showed that deactivation via polymerization can be important [23,65]. Addition of water to the feed can help to improve the activity and catalyst life [23]. In the present study dealing with bifunctional catalysis, no deactivation was observed in the first 24 h on stream.

The *n*-decane conversion yields obtained when increasing the reaction temperatures over SBA-15 catalysts with different amounts of HPW incorporated following the DS and IMP methods are shown in Fig. 8. Apparent *n*-decane reaction rates per HPW molecule at 210 °C are presented in Table 2. The *n*-decane conversion is not influenced much by the HPW loading (Fig. 8). In the DS series, the 30%HPW-DS and 40%HPW-DS samples are more active than the 20%HPW-DS sample (Fig. 8). When the activity is expressed per HPW molecule, 30%HPW-DS is the most active sample (Table 2). The existence of an optimum HPW loading at an intermediate HPW content was also observed by other authors [66]. In the present samples, the similarity in the activities of HPW-DS samples with 30 and 40 wt.% of HPW is consistent with the similarity in acidity observed with NH_3-TPD (Fig. 6). The impregnated samples show a gradual increase in the catalytic activity with the HPW content (Fig. 8). The apparent reaction rates per HPW molecule at 210 °C (Table 2) show some variation though little systematic. The catalytic activity per HPW molecule in IMP samples is systematically lower than that in DS samples, which is in agreement with the assumed better dispersion in DS samples and the lower numbers of acid sites determined via NH_3–TPD (see Section 3.1 above).

Table 2
Apparent reaction rate of decane conversion over HPW-IMP and HPW-DS bifunctional catalysts.

Catalyst	Apparent reaction rate[a] (mmol *n*-decane/mol HPW s)
20%HPW-DS	0.91
30%HPW-DS	1.31
40%HPW-DS	0.86
20%HPW-IMP	0.65
30%HPW-IMP	0.49
40%HPW-IMP	0.80

[a] At 210 °C.

A hydroisomerization catalyst is expected to maximize the skeletal isomerization yield while suppressing hydrocracking. The obtained *n*-decane isomerization yields on SBA-15-supported HPW catalysts are depicted in Fig. 9. The DS samples exhibit a similar behavior regardless of the HPW content (Fig. 9). With increasing *n*-decane conversion, the isomerization yield first increases and then decreases due to cracking of the isodecane molecules. The 30 and 40%HPW-DS samples show a high maximum *n*-decane isomerization yield of ~70%. The high isomerization yield is maintained up to high *n*-decane conversion levels. For the 20%HPW-DS sample, the isomerization yield is only slightly lower. A high yield of skeletal isomers from a long-chain *n*-alkane is one of the criteria defined by Weitkamp for bifunctional Y zeolite catalysis to be "ideal" [67]. In an ideal catalyst, the functions are well balanced and the acid-catalyzed conversions are rate determining. Additional criteria are the occurrence of high yields of multi-branched skeletal isomers, the occurrence of primary cracking, and the for-

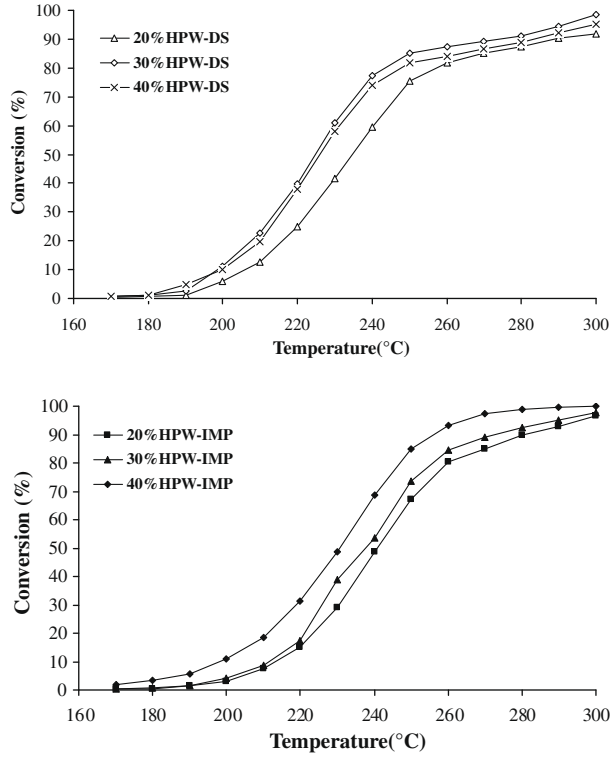

Fig. 8. Conversion of *n*-decane against reaction temperature over HPW-IMP and HPW-DS bifunctional catalysts.

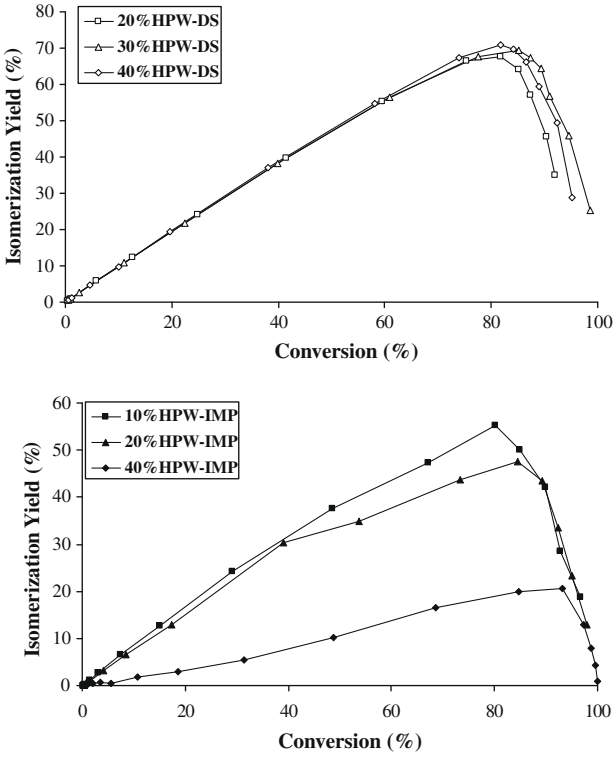

Fig. 9. *n*-Decane skeletal isomerization yield on bifunctional HPW/SBA-15 catalysts prepared according to DS and IMP methods against the *n*-decane hydroconversion.

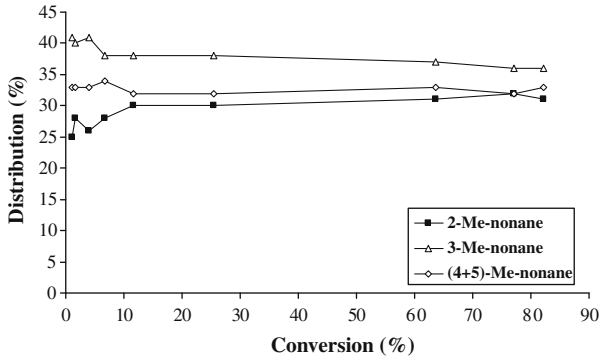

Fig. 10. Distribution of methylnonane positional isomers against *n*-decane conversion over bifunctional 30%HPW-DS catalyst.

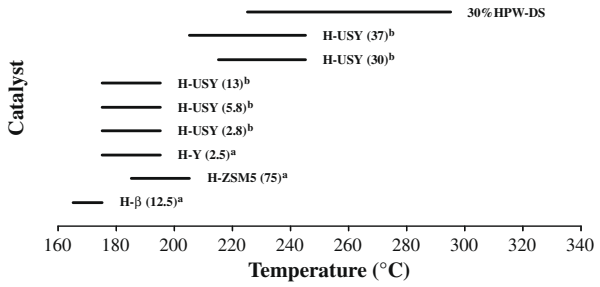

Fig. 11. Temperature interval where isomerization yields higher than 45% are obtained in the *n*-decane hydroisomerization over well-balanced bifunctional zeolite and HPW/SBA-15 catalysts (Si/Al atomic ratios of the zeolites are given within brackets).

mation of high amounts of branched cracked products [67]. For bifunctional Y type zeolites [63,64], the criteria for ideal bifunctional catalysis have been quantified as follows: total skeletal isomer yields exceeding 50%; multi-branched skeletal isomer yields exceeding 20%; formation of close to 200 mol of cracked products per 100 mol of long alkane cracked, and contents of isoalkanes in C_4 and heavier cracked product fractions exceeding 60%.

According to the isomerization yield criterion, in 0.5 wt.% Pt containing 20–40%HPW-DS catalysts the acidity and the hydrogenation–dehydrogenation activity are well balanced. The evolution of the distribution of positional methylnonane isomers with *n*-decane conversion is shown in Fig. 10. The formation of 2-methylnonane at low *n*-decane conversion levels is somewhat suppressed compared to that of the more centrally branched methylnonanes. This is a feature of skeletal isomerization via protonated cyclopropane reaction intermediates in the absence of shape selectivity effects [63,64].

While the catalytic activities of DS and IMP samples are rather similar (Fig. 8), the isomerization performances are significantly different (Fig. 9). In contrast to the DS samples, the isomerization yields of the IMP samples are lower and decrease with increasing HPW content (Fig. 9). The bifunctionality of catalysts in which the HPW is impregnated cannot be called "ideal". The stronger acidity of HPW-IMP samples revealed with NH_3-TPD (Fig. 7) offers an explanation for the deviation from ideality.

A number of zeolitic catalysts known for their excellent hydroisomerization performances were tested under the same reaction conditions. The temperature ranges in which the yields of *n*-decane isomerization over these bifunctional zeolites and the HPW catalysts of the present work exceed 45% are plotted in Fig. 11. Zeolites such as ZSM-5 and Beta which exhibit shape selectivity present a high activity (conversion at low reaction temperature) and show a maximum isomerization yield below 200 °C. The temperature window where the isomerization yield exceeds 45% is narrow and only ~20 °C wide for these two materials.

Bifunctional H-Y zeolite and a series of bifunctional ultrastable Y (H-USY) zeolites with a variety of dealumination levels were evaluated. The Pt-loaded H-USY zeolites with Si/Al ratios of 2.8–13 exhibit high *n*-decane hydroisomerization yields over 20 °C reaction temperature ranges. The high isomerization yield temperature window is broadened to 30 °C and 40 °C over bifunctional H-USY zeolites with Si/Al ratios of 30 and 37. The best hydroisomerization catalyst from the present study, viz. 30%HPW-DS, yields more than 45% of skeletal C_{10} isomers over a temperature window of 70 °C. This property of the 30%HPW-DS catalyst could be exploited for the conversion of *n*-alkane mixtures in order to simultaneously reach high skeletal isomerization yields of several *n*-alkanes with different chain lengths and reactivities.

The estimated concentration of acid sites in the 30%HPW/SBA-15 catalyst assuming three BrØnsted acidic OH groups per HPW molecule amounts to 0.3 mmol/g. This acid site concentration is similar to that of H-USY zeolite with a Si/Al ratio of 50. The H-USY zeolites tested, which had Si/Al ratios in the range 2.8–37 and thus had a higher acid site concentration, were more active than the 30%HPW-DS sample (Fig. 11).

Another important aspect of the *n*-alkane isomerization reaction is the possibility to obtain a large yield of multi-branched isomers. The evolution of the yield of monobranched isomers, dibranched isomers, and cracked products with increasing *n*-decane conversion on a 30%HPW-DS catalyst is shown in Fig. 12. Tribranched isodecanes were hardly formed and were neglected. Up to 40% *n*-decane conversion monobranching predominates. Dibranching and cracking are consecutive reactions. The yield of dibranched skeletal isomers peaks at ~25%. This value is superior to the values obtained on ultrastable Y zeolites and on the impregnated HPW/SBA-15 catalysts (Table 3).

Another criterion for ideal bifunctional catalysis is the occurrence of primary hydrocracking at low cracking conversions [67]. Fig. 13 shows the yield of cracked product fractions per 100 mol of *n*-decane cracked vs. the carbon number at 5% hydrocracking on the 30 wt.% HPW catalysts and H-USY(37) for comparison. A well-balanced catalyst should cause only primary cracking, yielding 200 moles of hydrocracked products per 100 moles of *n*-decane cracked. The total sum of cracked product yields for the 30%HPW-DS sample was 205 moles, close to 200, indicating that the catalyst is well balanced. The primary cracking is visualized in case of *n*-decane by the occurrence of equal molar yields of C_3 and C_7, as well as of C_4 and C_6. The 30%HPW-DS and -IMP samples exhibit primary cracking similar to the H-USY zeolite. The 30%HPW-DS catalyst is somewhat more selective for C_5 products formation than the Y

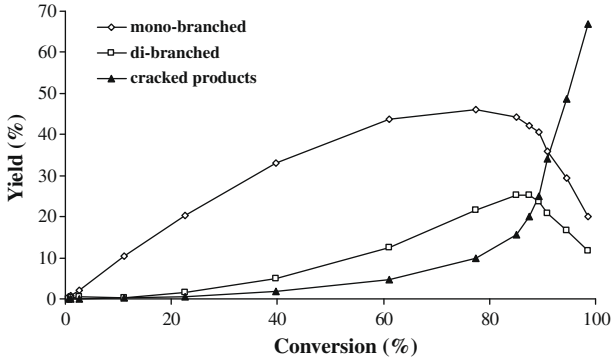

Fig. 12. Yield of mono- and dibranched isodecanes and cracked products in *n*-decane hydroconversion on a 30%HPW-DS catalyst.

Table 3
Maximum dibranched skeletal isomer yield from *n*-decane and the corresponding conversion level and temperature over bifunctional HPW/SBA-15 and reference zeolite catalysts.

Catalyst	Max. dibranched yield (%)	Conversion (%)	Temperature (°C)
20%HPW-DS	22.9	81.8	260
30%HPW-DS	25.3	85.1	250
40%HPW-DS	23.7	81.7	250
20%HPW-IMP	19.2	80.2	260
30%HPW-IMP	20.3	84.6	260
40%HPW-IMP	9.3	93.1	260
H-ZSM5 (75)	13.0	92.7	200
H-USY (2.8)	20.6	76.4	190
H-USY (30)	20.9	77.4	230
H-USY (37)	20.6	73.6	230

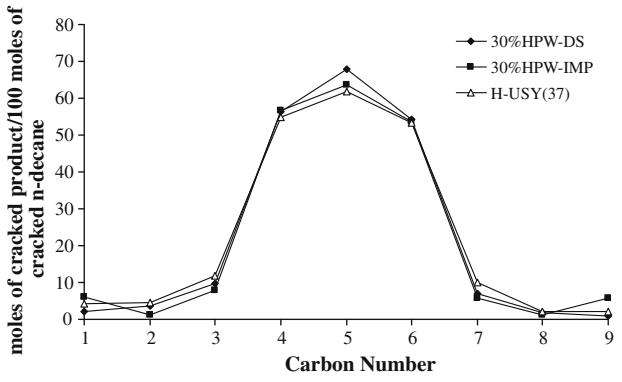

Fig. 13. Yield of cracked product fractions according to carbon numbers from *n*-decane hydrocracking on bifunctional 30%HPW/SBA-15 and H-USY zeolite catalysts at 5% cracking conversion.

Table 4
Content of branched molecules in carbon number fractions of cracked products (reaction temperature = 220 °C).

Catalyst	i-C_4 (%)	i-C_5 (%)	i-C_6 (%)	i-C_7 (%)
30%HPW-DS	71	74	75	82
30%HPW-IMP	72	80	81	84
H-USY(37)	68	75	78	80
H-USY(13)	73	76	76	88
H-USY(5.8)	71	76	74	85
H-USY(2.8)	70	74	74	87

type zeolite. The content of isoalkanes in the C_4-C_7 cracked product fractions is presented in Table 4. The formation of branched cracked products is a typical feature of decane hydrocracking in unconstrained environment [63,68]. The micropores present in the HPW-DS samples (Table 1) do not introduce molecular shape selectivity.

4. Conclusions

Tungstophosphoric acid was efficiently dispersed on a SBA-15 support via a direct synthesis method. The catalysts showed a homogeneous dispersion of the HPW molecules even at very high loadings such as 30 wt.%. The 30%HPW/SBA-15 sample loaded with 0.5 wt.% Pt had properties similar to those of an ideal bifunctional catalyst according to previously established criteria of high yields of skeletal isomerization and multi-branching, primary cracking, and high yields of branched cracked products. In *n*-decane conversion, a high isomerization yield is obtained over a wide reaction temperature range. The HPW-DS catalyst does not show any molecular shape selectivity. The product patterns are similar to those obtained on ultrastable Y zeolites. In hydroisomerization, the HPW catalyst is even superior to ultrastable Y zeolite with respect to optimal operating temperature window and multi-branched isomer yields. In comparative bifunctional HPW/SBA-15 catalysts in which the HPW is introduced via impregnation, the acid and hydrogenation–dehydrogenation functions are out of balance.

Acknowledgments

B.G acknowledges a grant from SBO-IWT. The authors acknowledge sponsoring in the frame of the following programs: SBO, GOA, IAP, FWO, and CECAT. J.A.M acknowledges the Flemish government for long-term structural funding (Methusalem).

References

[1] N. Mizuno, M. Misono, Chem. Rev. 98 (1998) 199.
[2] M.N. Timofeeva, Appl. Catal. A: Gen. 256 (2003) 19.
[3] T. Okuhara, Chem. Rev. 102 (2002) 3641.
[4] M. Misono, Chem. Commun. (2001) 1141.
[5] B.M. Devassy, S.B. Halligudi, S.G. Hegde, A.B. Halgeri, F. Lefebvre, Chem. Commun. (2002) 1074.
[6] G. Sunita, B.M. Devassy, A. Vinu, D.P. Sawant, V.V. Balasubramanian, S.B. Halligudi, Catal. Commun. 9 (2008) 696.
[7] S.M. Kumbar, G.V. Shanbhag, F. Lefebvre, S.B. Halligudi, J. Mol. Catal. A: Chem. 256 (2006) 324.
[8] N.G. Waghmare, P. Kasinathan, A. Amrute, N. Lucas, S.B. Halligudi, Catal. Commun. 9 (2008) 2026.
[9] A. Molnar, C. Keresszegi, B. Torok, Appl. Catal. A: Gen. 189 (1999) 217.
[10] Y. Izumi, K. Hisano, T. Hida, Appl. Catal. A: Gen. 181 (1999) 277.
[11] S.R. Mukai, M. Shimoda, L. Lin, H. Tamon, T. Masuda, Appl. Catal. A: Gen. 256 (2003) 107.
[12] S. Damyanova, L. Dimitrov, R. Mariscal, J.L.G. Fierro, L. Petrov, I. Sobrados, Appl. Catal. A: Gen. 256 (2003) 183.
[13] S.-Y. Yu, L.-P. Wang, B. Chen, Y.-Y. Gu, J. Li, H.-M. Ding, Y.-K. Shan, Chem. Eur. J. 11 (2005) 3894.
[14] P.M. Rao, A. Wolfson, S. Kababya, S. Vega, M.V. Landau, J. Catal. 232 (2005) 210.
[15] H. Kim, J.C. Jung, S.H. Yeom, K.-Y. Lee, J. Yi, I.K. Song, Mater. Res. Bull. 42 (2007) 2132.
[16] W. Kaleta, K. Nowinska, Chem. Commun. (2001) 535.
[17] A. Tarlani, M. Abedini, A. Nemati, M. Khabaz, M.M. Amini, J. Colloid Interf. Sci. 303 (2006) 32.
[18] H. Hamad, M. Soulard, B. Lebeau, J. Patarin, T. Hamiek, J. Toufaily, H. Mahzoul, J. Mol. Catal. A: Chem. 278 (2007) 53.
[19] C. Shi, R. Wang, G. Zhu, S. Qiu, J. Long, Eur. J. Inorg. Chem. (2005) 4801.
[20] L. Yang, Y. Qi, X. Yuan, J. Shen, J. Kim, J. Mol. Catal. A: Gen. 229 (2005) 199.
[21] C. Shi, R. Wang, G. Zhu, S. Qiu, J. Long, Eur. J. Inorg. Chem. (2006) 3054.
[22] J. Toufaily, M. Soulard, J.-L. Guth, J. Patarin, L. Delmotte, T. Hamieh, M. Kodeih, D. Naoufal, H. Hamad, Colloid Surf. A: Physicochem. Eng. Aspects 312 (2008) 285.
[23] J. Zhang, R. Ohnishi, Y. Kamiya, T. Okuhara, J. Catal. 254 (2008) 263.
[24] J. Wang, H.-O. Zhu, Catal. Lett. 93 (2004) 209.
[25] A. Bordoloi, F. Lefebvre, S.B. Halligudi, J. Catal. 247 (2007) 166.
[26] D.P. Sawant, A. Vinu, N.E. Jacob, F. Lefebvre, S.B. Halligudi, J. Catal. 235 (2005) 341.
[27] D.P. Sawant, M. Hartmann, S.B. Halligudi, Micropor. Mesopor. Mater. 102 (2007) 223.
[28] M. Labaki, M. Mokhtari, J.F. Brilhac, S. Thomas, V. Pitchon, Appl. Catal. B: Environ. 70 (2007) 151.
[29] K. Na, T. Okuhara, M. Misono, Chem. Commun. (1993) 1422.
[30] K. Na, T. Iizaki, T. Okuhara, M. Misono, J. Mol. Catal. A: Chem. 115 (1997) 455.
[31] B.B. Bardin, R.J. Davio, Top. Catal. 6 (1998) 77.
[32] N. Essayem, Y. Ben Taarit, P.Y. Gayraud, G. Sapaly, C. Naccache, J. Catal. 204 (2001) 157.
[33] W. Kuang, A. Rives, B.O.B. Tayeb, M. Fournier, R. Hubaut, J. Colloid Interf. Sci. 248 (2002) 123.
[34] N. Essayem, Y. Ben Taârit, C. Feche, P.Y. Gayraud, G. Sapaly, C. Naccache, J. Catal. 219 (2003) 97.
[35] W. Kuang, A. Rives, M. Fournier, R. Hubaut, Appl. Catal. A: Gen. 250 (2003) 221.
[36] A. Miyaji, T. Okuhara, Catal. Today 81 (2003) 43.
[37] A. Miyaji, R. Ohnishi, T. Okuhara, Appl. Catal. A: Gen. 262 (2004) 143.
[38] T. Sugii, R. Ohnishi, J. Zhang, A. Miyaji, Y. Kamiya, T. Okuhara, Catal. Today 116 (2006) 179.
[39] Y.-B. Gu, R.-P. Wei, X.-Q. Ren, J. Wang, Catal. Lett. 113 (2007) 41.
[40] J.C. Yori, J.M. Grau, V.M. Benitez, J. Sepulveda, Appl. Catal. A: Gen. 286 (2005) 71.
[41] J.A. Martens, P.A. Jacobs, in: J.B. Moffat (Ed.), Theoretical Aspects of Heterogeneous Catalysis, Van Nostrand Reinhold, New York, 1990, p. 52.
[42] A. Steynberg, M. Dry, Stud. Surf. Sci. Catal. 152 (2004) 506.

[43] J.M.F. Denayer, J.A. Martens, P.A. Jacobs, J.W. Thybaut, G.B. Marin, G.V. Baron, Appl. Catal. A: Gen. 246 (2003) 17.
[44] G.G. Martens, G.B. Marin, J.A. Martens, P.A. Jacobs, G.V. Baron, J. Catal. 195 (2000) 253.
[45] M.C. Claude, G. Vanbutsele, J.A. Martens, J. Catal. 203 (2001) 213.
[46] M.C. Claude, J.A. Martens, J. Catal. 190 (2000) 39.
[47] J.A. Martens, W. Souverijns, W. Verrelst, R. Parton, G.F. Gromet, P.A. Jacobs, Angew. Chem., Int. Ed. 34 (1995) 2528.
[48] J.A. Martens, P.A. Jacobs, J. Weitkamp, Appl. Catal. 20 (1986) 239.
[49] K. Flodstrom, V. Alfredsson, Micropor. Mesopor. Mater. 59 (2003) 167.
[50] M.J. Remy, D. Stanica, G. Poncelet, E.J.P. Feijen, P.J. Grobet, J.A. Martens, P.A. Jacobs, J. Phys. Chem. 100 (1996) 12440.
[51] W. Huybrechts, J. Mijoin, P.A. Jacobs, J.A. Martens, Appl. Catal. A: Gen. 243 (2003) 1.
[52] D. Zhao, J. Feng, Q. Huo, N. Melosh, G.H. Fredrickson, B.F. Chmelka, G.D. Stucky, Science 279 (1998) 548.
[53] Q. Huo, D.I. Margolese, U. Ciesla, P. Feng, P. Sieger, R. Leon, P. Petroff, F. Schüth, G.D. Stucky, Nature 368 (1994) 317.
[54] P.A. Jalil, N. Tabet, M. Faiz, N.M. Hamdan, Z. Hussain, Appl. Catal. A: Gen. 257 (2004) 1.
[55] E. Lopez-Salinas, J.G. Hernandez-Cortez, I. Schifter, E. Torres-Garcia, J. Navarrete, A. Gutierrez-Carrillo, T. Lopez, P.P. Lottici, D. Bersani, Appl. Catal. A: Gen. 193 (2000) 215.
[56] I.V. Kozhevnikov, K.R. Kloetstra, A. Sinnema, H.W. Zandbergen, H. van Bekkum, J. Mol. Catal. A: Chem. 114 (1996) 287.
[57] L.R. Pizzio, C.V. Caceres, M.N. Blanco, Appl. Catal. A: Gen. 167 (1998) 283.
[58] J.C. Groen, L.A.A. Peffer, J. Perez-Ramirez, Micropor. Mesopor. Mater. 60 (2003) 1.
[59] D. Zhao, J. Sun, Q. Li, G.D. Stucky, Chem. Mater. 12 (2000) 275.
[60] F.X. Liu-Cai, B. Sahut, E. Faydi, A. Auroux, G. Hervé, Appl. Catal. A: Gen. 185 (1999) 75.
[61] E.F. Kozhevnikova, I.V. Kozhevnikov, J. Catal. 224 (2004) 164.
[62] A. Lapkin, C. Savill-Jowitt, K. Edler, R. Brown, Langmuir 22 (2006) 7664.
[63] J.A. Martens, P.A. Jacobs, Zeolites 6 (1986) 290.
[64] J.A. Martens, M. Tielen, P.A. Jacobs, Zeolites 4 (1984) 218.
[65] S. Gao, J.B. Moffat, Catal. Lett. 42 (1996) 105.
[66] A.V. Ivanov, T.V. Vasina, V.D. Nissenbaum, L.M. Kustov, M.N. Timofeeva, J.I. Houzvicka, Appl. Catal. A: Gen. 259 (2004) 65.
[67] J. Weitkamp, Erdol Kohle Erdgas Petrochem. Brennstoffchem. 31 (1978) 13.
[68] A. Aerts, A. van Isacker, W. Huybrechts, S.P.B. Kremer, C.E.A. Kirschhock, F. Collignon, K. Houthoofd, J.F.M. Denayer, G.V. Baron, G.B. Marin, P.A. Jacobs, J.A. Martens, Appl. Catal. A: Gen. 257 (2004) 7.